Study on Meso-scale Grinding Surface Roughness and Sub-surface Quality of High Volume Fraction SiCp/Al2024 composites

Guangyan Guo
Liaoning University of Technology
Qi Gao (qqonline@163.com)
Liaoning University of Technology
Quanzhao Wang
Chinese Academy of Sciences
Yuanhe Hu
Liaoning University of Technology

Research Article

Keywords: SiCp/Al2024 composites, Two-dimensional simulation model, SiC particles, Surface roughness, Sub-surface quality

Posted Date: July 28th, 2021

DOI: https://doi.org/10.21203/rs.3.rs-742295/v1

Study on Meso-scale Grinding Surface Roughness and Sub-surface Quality of High Volume Fraction SiCp/Al2024 composites

Guangyan Guo[1]. Qi Gao[1]. Quanzhao Wang[2]. and Yuanhe Hu[1]

Received: /Accepted:

Abstract: In order to improve the surface grinding quality of high volume fraction aluminum matrix composites, the cutting tool models with different rake angles are established, the grinding process is simulated, and the material removal mechanism and the broken state of SiC particles are obtained. Through single factor experiment, the 60% volume fraction SiCp/Al2024 composites are ground by diamond grinding rod with 3mm diameter, the surface roughness (*Ra*) is measured, and the surface and sub-surface quality of SiCp/Al2024 composites with meso-scale grinding is investigated. Meanwhile, the influence mechanism of grinding depth (a_p) on surface quality is put forward, and the influence of different grinding depth on the fragmentation of SiC particles in sub-surface layer is discussed, which verifies the correctness of grinding simulation. The relevant research and theoretical model are of great significance to the study of grinding properties of composite materials.

Key words: SiCp/Al2024 composites. Two-dimensional simulation model. SiC particles. Surface roughness. Sub-surface quality

1. Introduction

SiCp/Al composites are metal matrix composites included with SiC particles and aluminum matrix. Due to its high heat conductivity coefficient, low thermal expansion coefficient, high strength, low density and other excellent characteristics [1], it has gradually become the focus of scholars. The material is widely used in including aerospace, precision instruments, optical and mechanical components and inertial devices, and so on [2-5]. In recent years, some scholars have studied the properties of metal matrix composite by means of grinding, so as to be better applied in practice.

A large number of scholars have explored the grinding mechanism of composite materials through grinding simulation. Zheng et al. [9] simulated the formation mechanism of surface defects in ultrasonic grinding of SiCp/Al composites. The results showed that the removal forms of SiC particles mainly include rolling in, breaking and pulling out. Zhang et al. [10] used the finite element analysis software (Abaqus) to simulate the process of grinding SiCp/Al composites with single Diamond Grits, and analyzed the influence of grinding speed and grinding depth on grinding force, the surface morphology and residual stress distribution of the workpiece after grinding were studied, which provided a reference for optimizing the processing parameters of SiCp/Al composites ground by diamond grinding wheel. Ma et al. [11] based on the Abaqus, the Johnson-Cook constitutive model was used to simulate the chip shape, chip shear angle and grinding force in high speed grinding of Ti6Al4V with different abrasive negative rake angle. Wang et al. [12] set up a two-dimensional finite

Po Jin
jinpo1015@163.com

Qi Gao
qqonline@163.com

Quanzhao Wang
1033550451@qq.com

Wenbo Li
653380100@qq.com

1. School of Mechanical Engineering and Automation, Liaoning University of Technology, Jinzhou, 121001,China.
2. Institute of Metal Research, Chinese Academy of Science, 110016

element model consisting of hard silicon carbide particles and soft aluminum matrix to study the milling process of SiCp/Al composites. The simulation results showed that the rotation, stretching, cracking, micro-fracture and cutting of sic are the main mechanisms of defect formation. The simulated machined surface morphology was compared with the milling surface profile, and a good correlation was obtained.

More and more scholars put forward the grinding mechanism of composite materials through the experimental method. Yu et al. [13] studied the form of grinding removal of high volume fraction SiCp/Al composites, analyzed the morphology and types of grinding surface defects and debris of SiCp/Al composites by SEM observation, and put forward its formation mechanism, a three-dimensional nonlinear finite element model of the grinding conditions in the plastic region of SiCp/Al Composites was established, and the effects of the radius and the depth of the blunt ball on the brittle-plastic transition of SiC particles in the hard reinforced phase of the composites were investigated. Guan et al. [14] used ELID grinding technology to conduct precision grinding experiments on 40% volume fraction SiCp/Al composites, studied the formation mechanism of machined surface, analyzed several typical grinding surface defects, and the grinding characteristics and removal mechanism of SiCp/Al composites were summarized. Wei et al. [15] prepared SiCp/Al6061 hybrid composites by vacuum hot pressing at 590 °C and 50 MPa, studied the microstructure and surface properties of the composites and their effects on the mechanical properties and thermal properties of the composites, and the machining performance was evaluated comprehensively. Sun et al. [16] studied the formation mechanism of particle damage in the processing of SiCp/Al composites and the effect of particle damage on chip formation. And based on the different degree of particle damage in the chip formation process, three new chip formation conceptual models with different fracture types were proposed to visually describe the chip formation process in SiCp/Al composites.

Overall, most scholars have used the method of macroscopic grinding low volume fraction SiCp/Al composites to study the effect of grinding force on the surface of ground materials, and established a simulation model to verify the correctness of grinding mechanism [17-19]. However, most scholars lacked of in-depth research on the sub-surface quality of high volume fraction SiCp/Al2024 composites during grinding. In order to simulate the grinding process of SiCp/Al2024 composites more accurately and observe the quality of the surface and the sub-surface, different grinding rake angles and different grinding depths are set by Abaqus software. Through the single-factor experiment method, the end surface grinding of the SiCp/Al2024 composite material with 60% reinforcement base particles is carried out, and the experimental results of the surface roughness are obtained, and the influence of the grinding depth on the surface and sub-surface quality after grinding is explained. The experimental results and the simulation results are mutually verified. Moreover, the influence of feed rate and grinding depth on the surface quality of the workpiece is discussed.

2. Experiment design

2.1 Experiment condition

SiCp/Al2024 composite is selected as the workpiece, the volume fraction of SiC particles is 60% , the particles are big and the hardness is high. And the average particle size of SiC particles is 40 μm, of which the smallest particle size is 20 μm and the largest particle size is 60 μm. The material characteristics of the workpiece are shown in Table 1.

Table 1 Workpiece material characteristics

Density ρ (kg/m^3)	2970
Thermal diffusivity (m^2/s)	9.93×10^{-5}
Specific heat (J·kg^{-1}·K^{-1})	689
Thermal conductivity (W·m^{-1}·K^{-1})	203
Young´s modulus (GPa)	206
Poisson´s ratio	0.24
Thermal expansion coefficient (°C^{-1})	7.98×10^{-6}

When n is 14000 r/min, v_w is 0.003 m/min, and a_p is 15 μm, the Matlab Software is used to simulate the groove of end surface grinding of SiCp/Al composite, and the simulation result is shown in Figure 1(a). Meanwhile, under the same grinding parameter

conditions, a grinding experiment is performed on the workpiece, and the microstructure of the workpiece is obtained as shown in Figure 1(b). Therefore, the simulation results and the observed experimental results mutually verify each other, so this series of experimental studies is feasible.

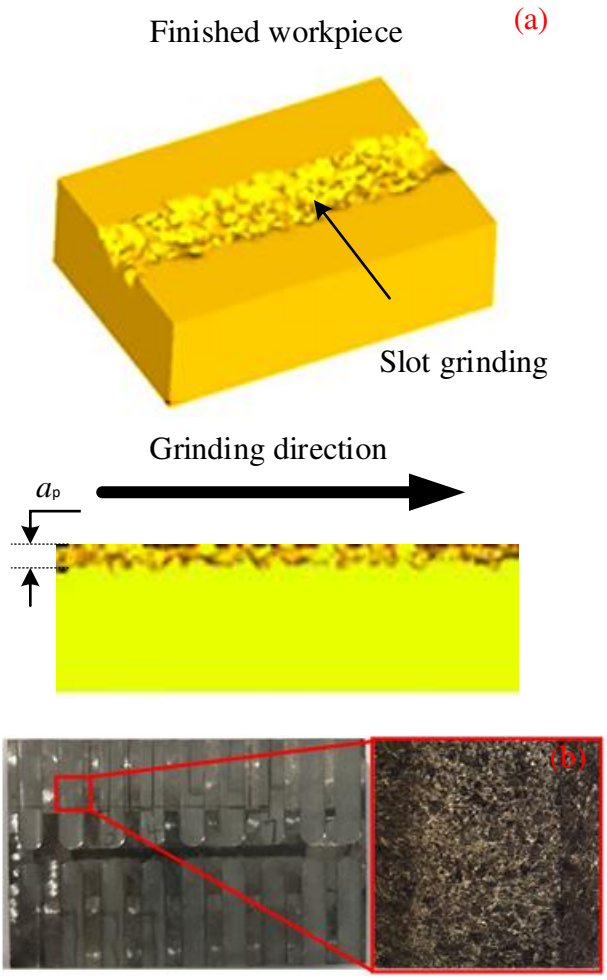

Fig. 1 Surface morphology of machined workpiece (a) Simulation of groove surface shape after machining (b) Morphology and microstructure of real surface

As shown in Figure 2, the micro-grinding experiment platform is set up. The machining equipment is a Beijing precision Carver400GA CNC machine, the size of the worktable is 490 × 430mm, the spindle speed is up to 30000rpm, and the positioning accuracy of x/y/z axis is 0.008/0.008/0.006 mm, x/y/z axis repetitive positioning accuracy is 0.005/0.005/0.005 μm, maximum grinding rod feed rate is 6 m/min. SiCp/Al2024 composites are ground by using electroplated diamond grinding rod. The grinding head diameter and grinding rod shank diameter is 3mm, the grinding rod mesh number is #150, and the average abrasive grain strength is 200 μm. In addition, the boron nitride is added to the grinding rod to improve the heat resistance and prevent sand loss during grinding, thus extending the service life effectively.

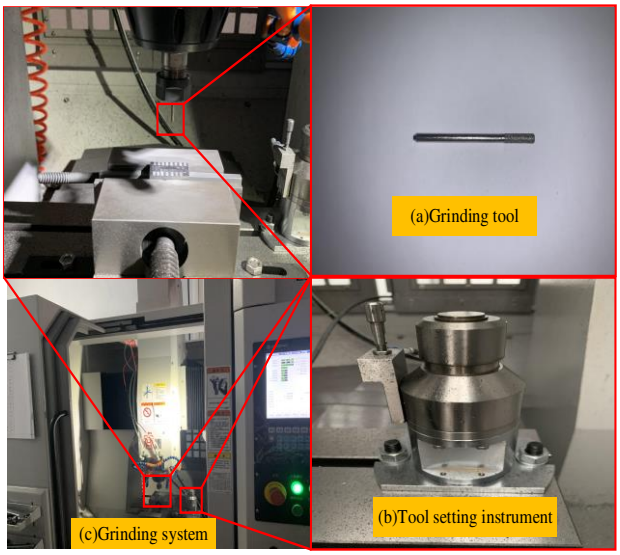

Fig. 2 Schematic diagram of grinding experiment system

The end surface grinding experiments are carried out on the Carver 400 high-precision engraving machine, and the Zeiss SIGMA 500 scanning electron microscope is used to observe the surface and subsurface quality of the processed workpiece. The equipment is shown in Figure 3.

Figure 3 Schematic diagram of the microscope system

2.2 Experimental procedure

Through comparative analysis, the grinding mechanism of SiCp/Al2024 composite material is discussed. Simultaneously, in order to obtain more accurate experimental results, the grinding experiment adopts the dry grinding method [20-22], and the grinding process parameters are shown in Table 2.

Table 2 Grinding process parameters

Conditions	Dosage
Grinding rod type	electroplated diamond grinding rod #150
Grinding type	End surface grinding
Spindle speed n/(r/min)	14000
Feed rate v_w /(m/min)	0.003、0.005、0.007
Grinding depth a_p/(mm)	0.01、0.015、0.02、0.025、0.03
Grinding process conditions	Drying grinding

In the grinding process, the spindle speed is 14000 r/min, the grinding depth is 10 μm - 30 μm, and the feed rate is 0.003, 0.005, and 0.007 m/min. The specific experimental data design is shown in Table 3.

Table 3 Grinding experiment Scheme

Number	n/(r/min)	v_w/(m/min)	a_p/ (μm)
1	14000	0.003	10
2	14000	0.003	15
3	14000	0.003	20
4	14000	0.003	25
5	14000	0.003	30
6	14000	0.005	10
7	14000	0.005	15
8	14000	0.005	20
9	14000	0.005	25
10	14000	0.005	30
11	14000	0.007	10
12	14000	0.007	15
13	14000	0.007	20
14	14000	0.007	25
15	14000	0.007	30

Figure 4 shows a schematic diagram of the grinding rod end surface grinding SiCp/Al2024 composite material. After the grinding rod is used to determine the grinding depth along the F_z direction, the electroplated diamond grinding rod is uniformly ground from one side of the workpiece to the other at a constant feed rate and spindle speed. The yellow area in Figure 4 is the area where the grinding has been completed. This area is mainly processed by diamond particles on the end face of the grinding bar. Because the shape of the grinding rod is cylindrical and the grinding is continuous, a complete groove is left on the workpiece after grinding. The sub-surface quality is detected after the wire cutting in the grinding feed direction, and the surface of the groove is the testing position. When the spindle speed is constant, the surface quality and sub-surface quality of the workpiece will be greatly affected by changing the grinding depth of the grinding bar or the feed rate of the workpiece. Therefore, this experiment uses 15 groups of

single factor experiments to illustrate the degree of influence of different grinding parameters on the quality of the first two. Meanwhile, when different grinding parameters are used to remove the workpiece as a whole, the removal ways of SiC reinforced particles and aluminum matrix are also different.

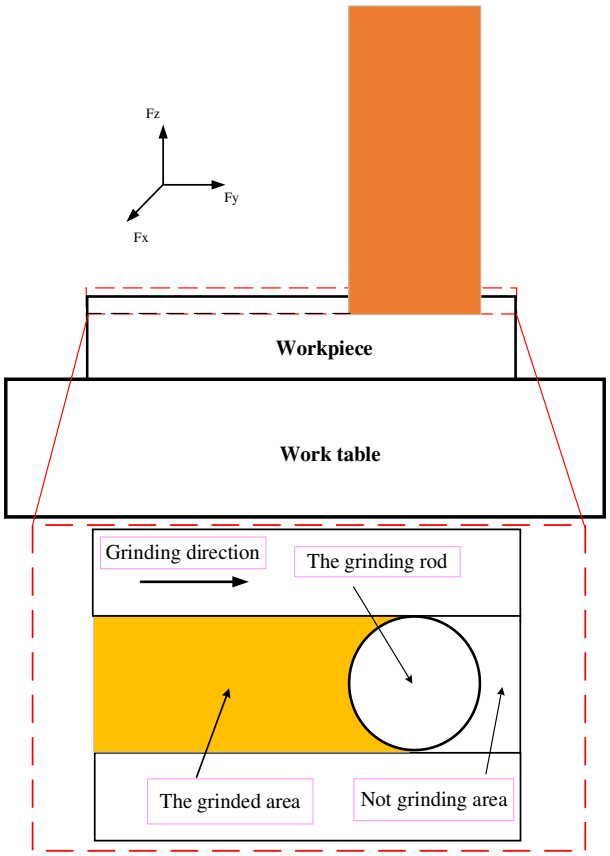

Fig. 4 Schematic illustration of face grinding

3. Establishment and analysis of the simulation

3.1 Finite element model

Fig. 5 is a finite element model for grinding 60% SiC reinforced aluminum matrix composites. In this model, the transverse direction is X and the longitudinal direction is Y. The whole model consists of two parts, one is SiCp/Al composite model, the other is single grain diamond tool model. In the simulation software, the workpiece is set as a two-dimensional rectangle with a length of 0.08 mm and a width of 0.04 mm. And the SiC particles are simulated to be many different size circles with radius between 1 μm and 5 μm. The total area of all circles accounts for 60% of the total area of the rectangle, which is consistent with the 60% volume fraction of SiC particles. In addition to the reinforced particles, the remaining part of the workpiece is aluminum matrix. The overall shape of the workpiece is a large number of circular areas surrounded by a rectangle. Furthermore, the grinding rake angle is more than 90° in the tool grinding, so the tool is simplified into a right-angle trapezoid. And a circular arc with a radius of 1μm is set at the rake angle of the tool according to the parameters of actual grinding rod.

In the process of simulation modeling, the workpiece is divided into 11252 units, in which the area occupied by SiC particles is divided into 7808 units, and the aluminum matrix is divided into 3444 units. Because the removal mode of the composite is mainly determined by the SiC particles, the SiC particles are divided into fine grids, so the number of units formed in the region occupied by SiC particles is more than twice as large as that occupied by aluminum matrix. In addition, due to the high hardness of diamond particles, the tool in the simulation is set to a rigid body, so it does not require mesh division.

Similarly, due to the grinding process of slip and other aspects of the characteristics, it is necessary for the workpiece and tools for a variety of constraints in this simulation process. Firstly, for the workpiece, the bottom and most of the left and right sides are constrained (the red triangle in the figure is the constraint symbol) to ensure that the simulation is running properly.Secondly, it is given an initial velocity to the left which makes it cut continuously from right to left in the horizontal direction in the motion setting of the tool.

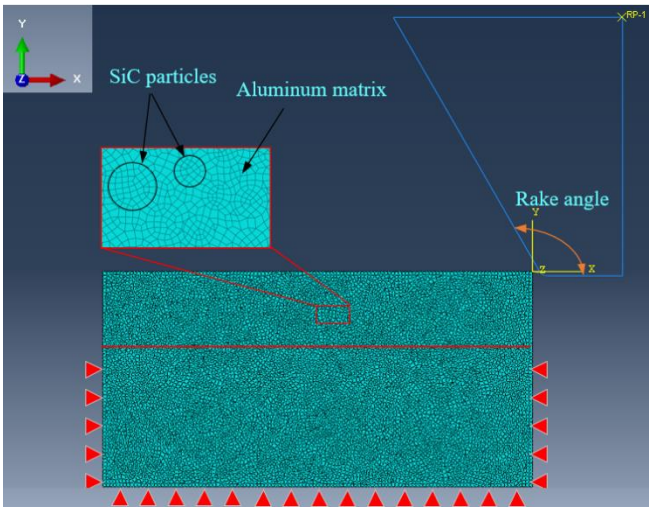

Fig. 5 Finite element model of grinding SiCp/Al

3.2 Matrix material

According to Hooke's law, SiC particles in SiCp/Al2024 composites are defined as perfectly elastic materials. In this paper, the model of SiC composite is established, and the brittle fracture and extrusion dislocation of SiC particles are analyzed by finite element method. In the process of rod grinding composite materials, relative motion occurs, which causes friction resistance, so the temperature of the workpiece increases greatly, resulting in large strain on the material to be processed. Johnson and Cook [23] proposed Johnson-Cook (J-C) constitutive equation based on the simulation of matrix material. In addition, Akbari et al [24] improves the Johnson-Cook damage limit criterion. Johnson-Cook constitutive model can accurately describe the stress-strain relationship of metal materials under large strain rate. The three parameters of strain hardening, strain rate hardening and temperature softening are combined to express the deformation of the material in the process of machining.The material constitutive model can be expressed as:

$$\sigma = (A + B\varepsilon_{\mathrm{p}}^{\mathrm{n}})\left[1 + C\ln\left(1 + \frac{\varepsilon}{\varepsilon_0}\right)\right]\left[1 - \left(\frac{T - T_0}{T_{melt} - T_0}\right)^m\right] \quad (1)$$

Where, σ is the Misses flow stress, A is the initial yield stress, B is the strain hardening parameter of the material, C is the strengthening parameter of material strain rate, n is the hardening index, m is the thermal softening index of the material. T_{melt} is the temperature of the material's melting point. T_0 is room temperature. Among them, A, B, C, n and m need to be determined by the separation of the Hopkinson pressure bar (SHPB) experiment, and the material parameters are shown in Table 4.

Table 4 J-C constitutive model parameters of SiC/Al Composites

A(MPa)	B(MPa)	C	n	m	T_{melt}(℃)	T_0(℃)
265	526	0.06	0.325	1.95	720	20

The Johnson-cook separation criterion is used to produce the failure when the strain at the integration node reaches a predetermined critical value. When the failure parameter (ω) is greater than one, the failure of the material can be assumed. If all points fail in the model, the material mesh will be cut off and detached from the workpiece. The failure parameter can be written as:

$$\omega = \sum \frac{\Delta\varepsilon \frac{\mathrm{p}l}{f}}{\varepsilon \frac{pl}{f}} \quad (2)$$

Where, $\Delta\varepsilon \frac{pl}{f}$ is the change in strain per incremental stepper unit time, $\varepsilon \frac{pl}{f}$ refers to the failure strain, which is affected by unit strain rate, hydrostatic stress Misses deviation ratio and unit temperature.

$$\varepsilon \frac{pl}{f} = \left[D_1 + D_2 \exp\left(D_3 \frac{p}{q}\right)\right]\left[1 + D_4 \ln\left(\frac{\varepsilon \frac{pl}{f}}{\varepsilon_0}\right)\right] \times (1 + D_5\theta) \quad (3)$$

Where M_1—M_5 is the coefficient of failure, and the parameters are shown in Table 5.

Table 5 J-C model failure parameter of SiC/Al Composites

M_1	M_2	M_3	M_4	M_5
0.226	0.14	-1.6	0.022	0

3.3 Analysis of the simulation results

The influence of different grinding rake angle on the simulation results should be considered because the grinding rod is rotary grinding and the distribution of diamond particles is not uniform on the grinding rod. In this simulation, the tool rake angle is set to 105°, 120°, 135° and 150°, respectively, to get more accurate simulation results to illustrate the removal of composite materials. When n is 14000r/min, v_w is 0.005m/min and a_p is 20 μm and 30 μm respectively, the simulation parameters are shown in Table 6.

Table 6 Simulation parameters

a_p/μm	20	20	20	20	30
Angle/°	105	120	135	150	105

When n = 14000r/min, v_w = 0.005m/min, a_p = 20μm and the tool rake angle is set at 105°, the two-dimensional simulation model of diamond bar grinding SiCp/Al2024 composites is shown in Fig. 6(a). It can be seen from the diagram that the removal mode of aluminum matrix is plastic removal, while the removal mode of silicon carbide particles is mainly particle crushing and particle pulling out. When the bottom of the tool cuts through the top or upper middle parts of the particles, the particles are subjected to larger stress transfer to produce cracks until they are broken, and the surface quality is affected to some extent. When the bottom surface of the tool cuts through the middle or lower middle parts of the particles, the particles are pulled out as a whole, forming large pits on the processed surface, making the surface quality worse.

When a_p increases from 20 μm to 30 μm, the two-dimensional simulated topography is shown in Figure 6(b). The figure shows that the removal of aluminum matrix is still plastic removal, while the removal of silicon carbide particles is particle disintegration, particle extraction and particle crushing. When the grinding depth increases, the resistance of the workpiece will increase, and the stress will transfer to the sub-surface layer, which will make the particles bear more stress, so some particles will be broken, therefore, it is necessary to study the sub-surface quality.

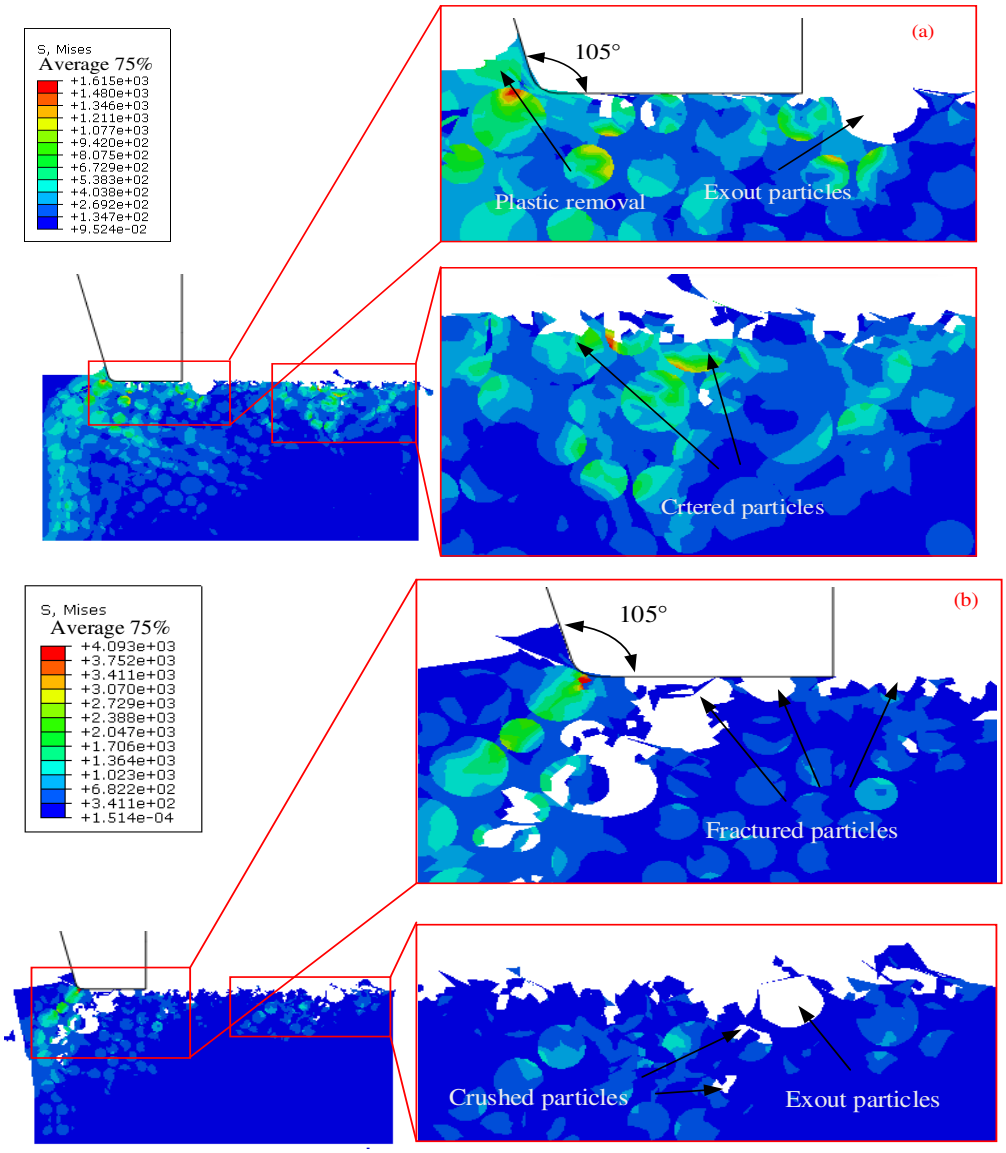

Fig. 6 Two-dimensional simulation topography at different grinding depths (a) a_p=20 μm (b) a_p=30 μm

When n = 14000r/min, v_w = 0.005m/min, a_p = 20μm, and the tool rake angle is set to 120°, the two-dimensional simulation model of diamond grinding rod grinding SiCp/Al2024 composite is shown in Figure 7(a). When the rake angle of the tool increases from 105° to 120°, it is obvious that the number of particles crushed increases indirectly by the tool, and the maximum stress of the process reaches 3 × 10^3 MPa. When the tool rake angle increases, the extrusion pressure of the tool rake face increases to the workpiece, so the stress of the particle increases inside the workpiece, which leads to the increase of the number of particles crushed indirectly. When the cutter moves to the end of the workpiece, the cutter tears the workpiece. The depth of tearing is shown in Figure 7(a). The internal tensile stress of the workpiece to the end is less than the tensile stress of the workpiece to other positions. When the shearing force generated by the tool on the workpiece is greater than the tensile stress of the workpiece to the end, it will cause partial tearing of the end.

When the three parameters of grinding remain unchanged, and the rake angle of the tool increases to 135°, the two-dimensional grinding simulation model of the workpiece is shown in Figure 7(b). It can be seen from the figure that the surface quality of the processed area has significantly deteriorated, because the processed surface of the workpiece has a large number of pits formed by the collapsed SiC particles. Meanwhile, as the rake angle of the tool increases, the shear force on the rake face of the workpiece increases, so the stress on the SiC particles inside the workpiece increases. When the stress exceeds the bearing capacity of the reinforcing particles, SiC particles will break up, resulting in a decrease in the quality of the sub-surface layer. When the tool angle is 135°, the shear stress on the rake face of the tool on the workpiece instantly reaches the maximum value of 7.5×10^3 MPa. When the depth of the tool tearing the end of the workpiece reaches the maximum, the depth is 2.5 times the depth of the tool tearing the workpiece with a 120° rake angle.

Under the premise that the various grinding parameters remain unchanged, when the rake angle of the tool is increased to 150°, the two-dimensional grinding simulation model of SiCp/Al2024 composite is shown in Figure 7(c). Simultaneously, as the shear stress of the tool on the workpiece continues to increase, the crushed reinforcement particles continue to increase, so the surface quality and sub-surface quality become worse. Although the longitudinal shear force is increased, the transverse shear force is reduced compared to Fig. 7(b), so the tearing depth of the tool to the end of the workpiece is basically the same as that of Fig. 7(a).

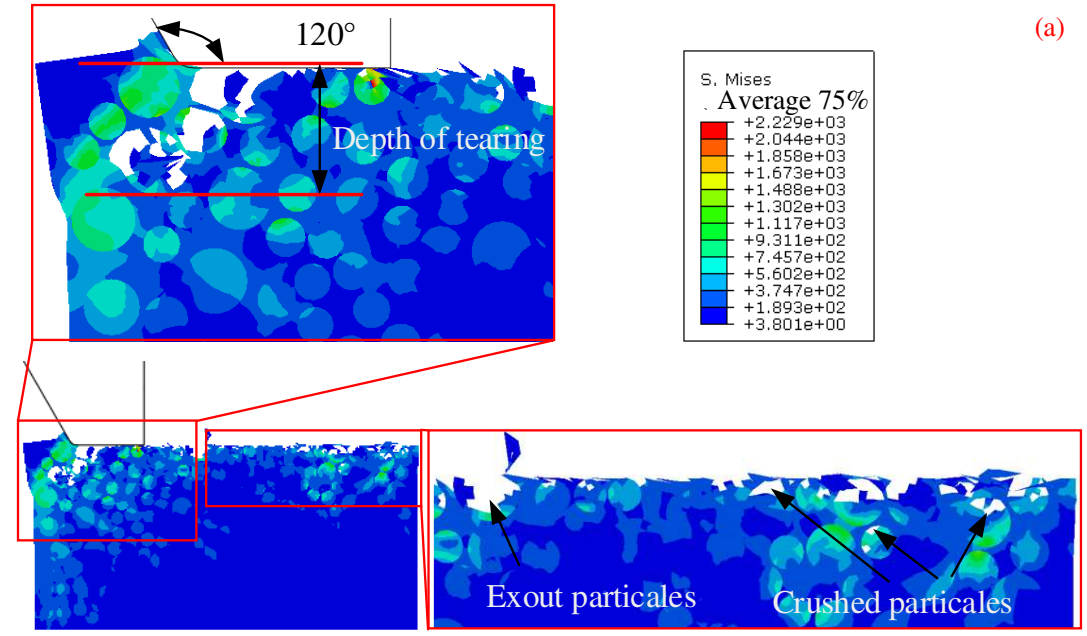
(a)
120°
Depth of tearing
S, Mises
Average 75%
+2.229e+03
+2.044e+03
+1.858e+03
+1.673e+03
+1.488e+03
+1.302e+03
+1.117e+03
+9.311e+02
+7.457e+02
+5.602e+02
+3.747e+02
+1.893e+02
+3.801e+00
Exout particales
Crushed particales

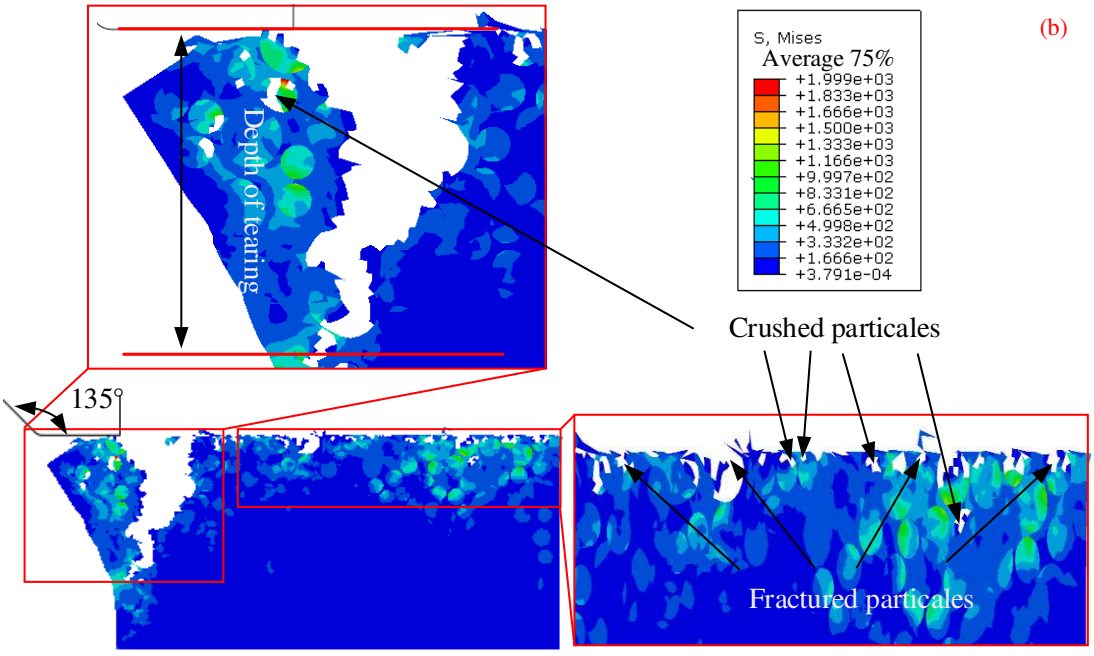
(b)
Depth of tearing
S, Mises
Average 75%
+1.999e+03
+1.833e+03
+1.666e+03
+1.500e+03
+1.333e+03
+1.166e+03
+9.997e+02
+8.331e+02
+6.665e+02
+4.998e+02
+3.332e+02
+1.666e+02
+3.791e-04
Crushed particales
135°
Fractured particales

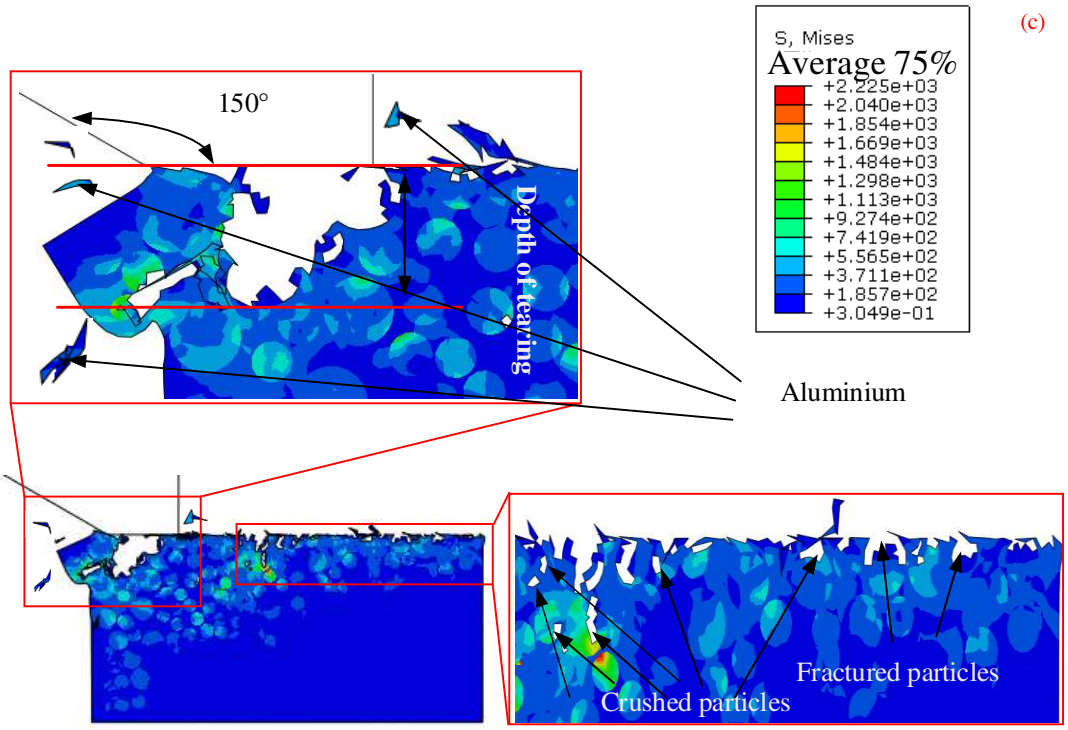

Fig. 7 Two-dimensional simulation topography under different rake angles (a) The angle is 120° (b) The angle is 135° (c) The angle is 150°

4. Results and discussion of experiments

4.1 Experimental results

Since the grinding depth (a_p) has a greater influence on the surface roughness (Ra), the surface quality is studied under the change of grinding depth. A 3 mm diameter electroplated diamond grinding rod is used to grind the SiCp/Al2024 composite material on the Carver 400 precision engraving machine. According to the experimental scheme in Table 3, the experimental results of surface roughness are obtained, as shown in Fig. 8.

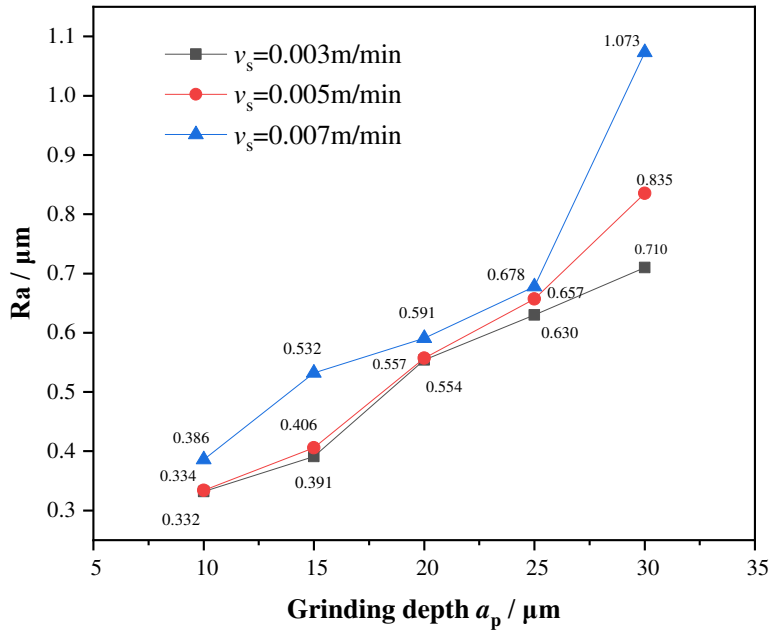

Fig. 8 Surface roughness values under different grinding parameters

It can be seen from Figure 8 that when the spindle speed (n) and the grinding rod feed rate (v_w) remain unchanged, as the grinding depth increases, the surface roughness also increases. When the grinding depth increases, the normal grinding force and the tangential grinding force increase at the same time, and the number of broken SiC particles on the surface of the workpiece increases, so the surface roughness is on the rise. When v_w = 0.003 m/min, when a_p increases from 10 μm to 30 μm, the value of *Ra* rises from 0.332 μm to 0.71 μm. When a_p increased from 15 μm to 20 μm, the *Ra* increased the most, and its value rose from 0.391 μm to 0.554 μm. When v_w = 0.005 m/min, under the same a_p increment condition, the value of *Ra* rises from 0.334 μm to 0.835 μm. When v_w = 0.007 m/min, under the same a_p increment condition, the value of *Ra* rises from 0.386 μm to 1.073 μm. Under the above two feed rates, when a_p increases from 25 μm to 30 μm, the *Ra* increases the most, with increments of 0.178 μm and 0.395 μm respectively. In general, when a_p exceeds 25 um, the *Ra* increases significantly, and it is recommended to control the a_p.

4.2 Analysis of experimental results based on 3D nephogram

The Zeiss SIGMA 500 scanning electron microscope is used to detect the microstructure of the three groove-shaped processed surfaces, and the corresponding 3D nephograms are formed to better propose the surface mechanism of the processed workpiece. Under n = 14000 r/min, v_w = 0.007 m/min, and a_p of 10 μm, 20 μm and 30 μm respectively, the local microstructure and 3D nephogram of the machined surface are shown in Figure 9.

In Figure 9(a), the value of *Ra* is 0.386 μm. It can be seen from the part showing the microstructure that more pits and shallower gullies are left on the processed surface. As the surface roughness is low, the pits are formed by fragmentation of SiC particles. The aluminum matrix is a plastic material, and its removal method is plastic removal, so the tool abrasive grains leave scratches on the matrix and form a shallower ravine. However, because the value of a_p is small, the depth of the ravine is small. So the surface quality is not greatly affected. And it can be fully verified from the 3D nephogram that there are shallow ravines and a few pits on the surface, and the surface quality is good.

In Figure 9(b), the value of *Ra* is 0.591 μm. It can be seen from the microstructure display that most of the pits are deep, so the pits here are caused by a small number of SiC particles broken and most SiC particles pulled out as a whole. This is fully verified by the corresponding 3D nephogram. Besides, the 3D nephogram shows that very few of the spikes are formed on machined surfaces after plastic removal of the aluminum matrix or SiC particles are broken.

In Figure 9(c), the value of *Ra* is 1.073 μm. From the pits in the 3D nephogram, it can be seen that there are three forms of SiC particles: breaking, pulling out and crushing, and most of the particles are already incomplete. In addition, due to the large value of ap, the scratches produced are deeper, and multiple deep gullies have been revealed, causing serious damage to the surface quality. At this time, the Ra of the processed workpiece has reached the maximum value.

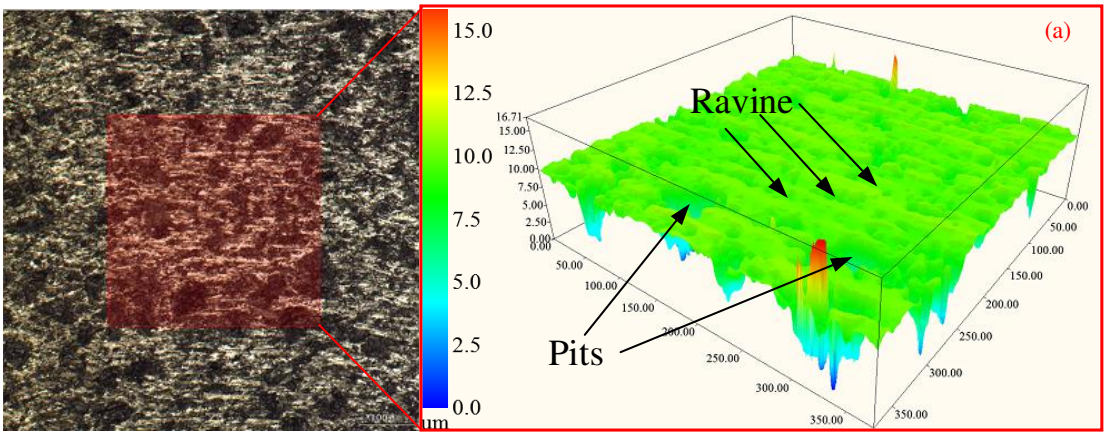

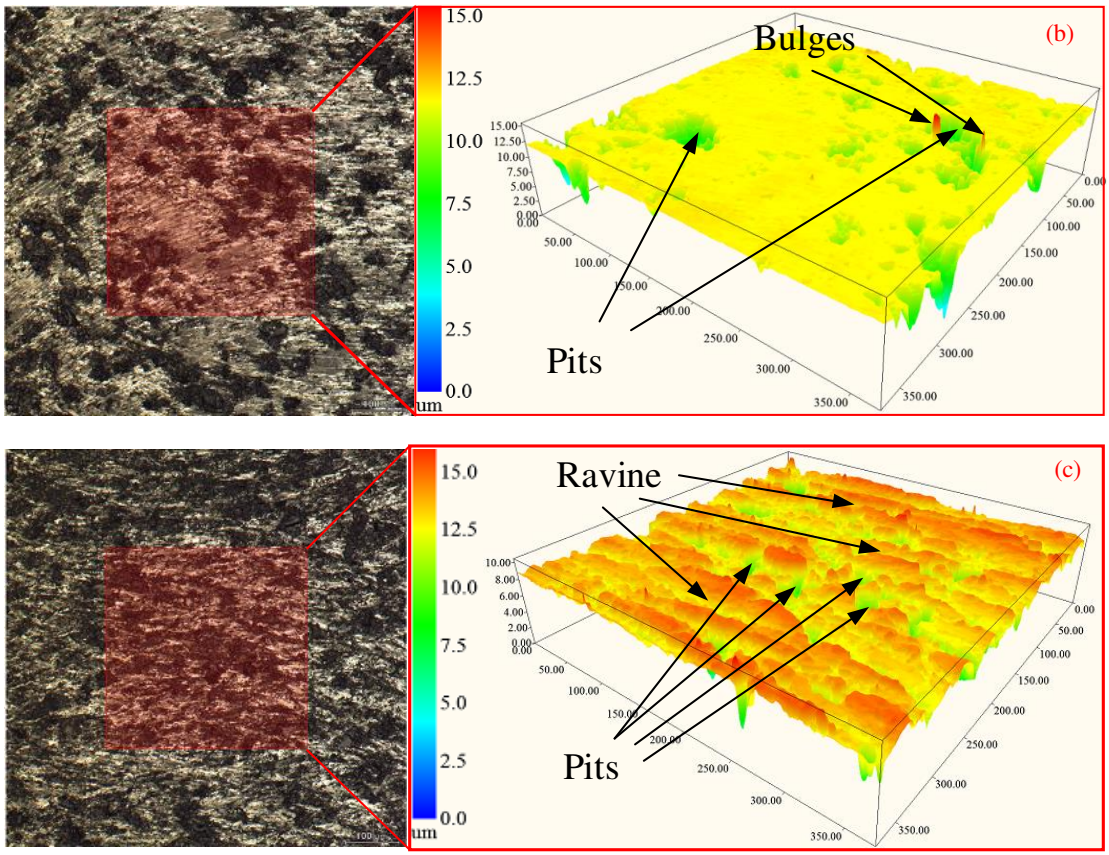

Fig. 9 Surface roughness microstructure and 3D nephogram (a) a_p=10 μm (b) a_p=20 μm (c) a_p=30 μm

From the perspective of experimental results, the collapse of particles, pull-out of particles and the depth of scratches are all important factors to affect the surface quality. To improve the surface quality of processed workpieces, smaller SiC particles can be selected as reinforcement particles. In terms of the effect of ap on the surface quality, the multi-step processing can lower the value of *Ra*.

4.3 Analysis of experimental results based on sub-surface microstructure

In order to study the quality of the sub-surface layer, the experimental parameters are set, as shown in Table 7. After the grinding is completed, wire cutting is performed along the grinding feed direction and the quality of the sub-surface layer is tested. And the experimental results are shown in Figure 10.

Table 7 Experimental parameter

Serial number	Experimental factors		
	n (r/min)	v_w (m/min)	a_p (μm)
1	14000	0.005	10
2	14000	0.005	20
3	14000	0.005	30

As shown in Figure 10(a), in the case of a_p = 10 μm, the thickness of the damaged layer of the workpiece is small, and some cracks and a small amount of voids will occur close to the surface; Meanwhile extremely a few cracks and voids will also appear at the position far from the processed surface. When the end face of the grinding rod grinds the surface of the workpiece, the closer it is to the surface, the greater the stress transfer and the better the stress transfer effect. Therefore, the farther away from the surface, the greater the degree of damage. When the end face of the grinding rod grinds the surface of the workpiece, the closer it is to the surface, the greater the stress transfer and the better the stress transfer effect, so the closer the surface is, the greater the degree of damage. Since the strain required to form a cavity is greater than the strain required to form a crack, most of the cavity is formed close to the surface. Similarly, as the distance from the surface gets farther and farther, fewer cracks are

produced.

Compared with Fig. 10(a), the thickness of the damaged layer of the workpiece is increased, and the length of the crack generated close to the surface is also increased in Fig. 10(b). Meanwhile, the number of cavities close to the processed surface also increases. Under the condition of a_p = 20 μm, because the normal grinding force on the end face of the grinding rod increases, the strain increases on the workpiece, which leads to a larger length of cracks and most cavities near the surface layer. In general, the degree of damage to the sub-surface layer is significantly greater than the result shown in Figure 10(a).

When the grinding depth is 30 μm, the sub-surface damage of the workpiece is shown in Figure 10(c). The processed surface quality is poor, and the quality of the sub-surface layer is lower than the above two cases. In the place closer to the machined surface, the number of cracks increases while accompanied by a large number of cavities. A large number of cracks are also generated in the place far away from the processed surface, and the number of voids is also significantly increased compared to Figure 10(a) and Figure 10(b).

When the spindle speed and feed rate are constant, the normal grinding force of the end face of the grinding rod on the workpiece increases with the increase of a_p, so the stress on the subsurface layer increases. For SiC particles with fragile properties, when it is subjected to a large enough stress, the particles will first crack until the crack penetrates the particle itself, and finally collapse. Therefore, when the spindle speed and the feed rate are unchanged, a_p is inversely proportional to the quality of the sub-surface layer. The larger the a_p, the worse the quality of the sub-surface layer. Because the stress transmission gradually decreases with the increase of distance in this material, the farther away from the surface, the better its quality. And because the stress required to form the cavity is greater, the number of cavities formed closer to the processed surface is more than the number of cavities formed at a position farther from the processed surface. When the stress is not enough to break the SiC particles, the cracks are left in the sub-surface layer of the SiCp/Al composite material. The length of the crack is determined by the distance between the particle location and the machined surface. The longer the distance between the two, the shorter the crack length, and vice versa.

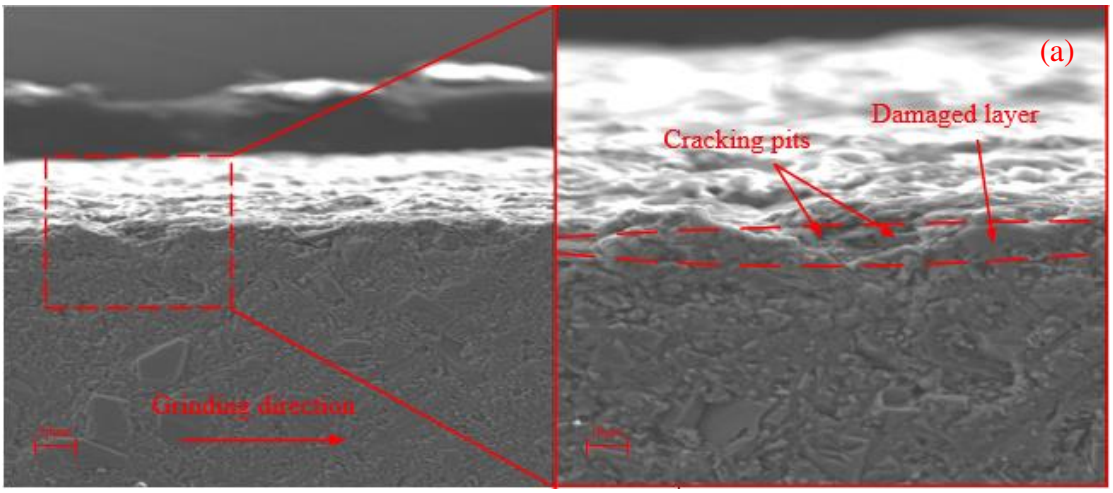

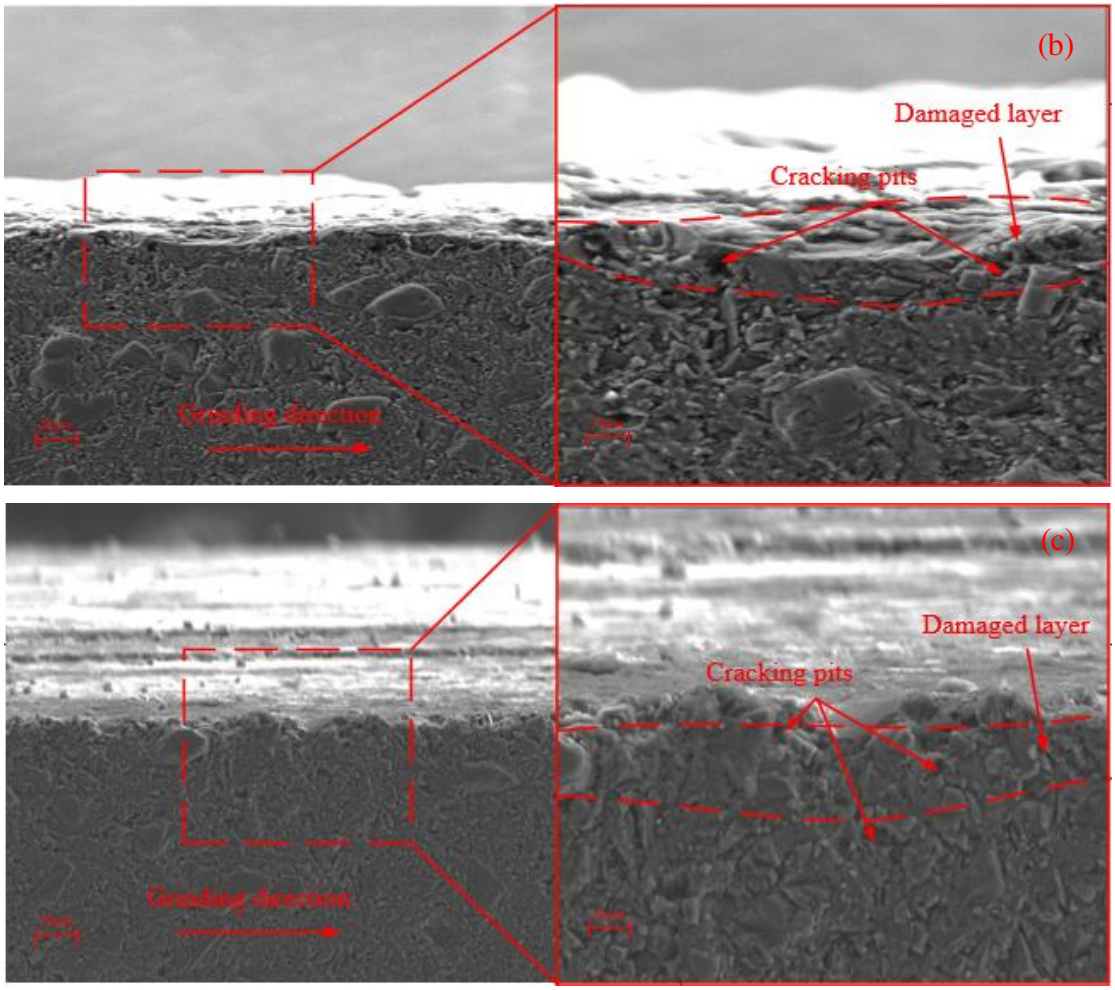

Fig. 10 Sub-surface microstructure of SiCp/Al composite (a) a_p = 10 μm (b) a_p = 20 μm (c) a_p = 30 μm

5. Conclusions

(1) Based on the grinding experiment of SiCp/Al2024 composite material (SiC particles accounted for 60% by volume fraction), a grinding rod end face grinding experiment platform is built. And different grinding parameters are selected for 15 groups of single factor experiments, and Ramax is obtained as 1.073 μm, the Ra_{min} is 0.332 μm. Besides, the degree of influence of grinding depth on surface roughness is greater than the degree of influence of feed rate on surface roughness.

(2) Two-dimensional simulation models with four different angles of 105°, 120°, 135° and 150° are established, and the grinding process is simulated, and the material removal mechanism and the crushing state of SiC particles are obtained.Among, when the rake angle of the tool is 135°, the tearing depth of the tool reaches the maximum at the end of the workpiece.

(3) Under the conditions of n = 14000 r/min, v_w = 0.007 m/min, and grinding depths of 10 μm, 20 μm, and 30 μm respectively, the Ra values are 0.386 μm, 0.591 μm, and 1.073 μm. As the grinding depth continues to increase, the surface quality continues to decline.

(4) Under the grinding parameters of n = 14000 r/min, v_w = 0.005 m/min, and a_p of 10 μm, 20 μm and 30 μm, the microstructure of the subsurface layer is detected. When the spindle speed and feed rate are unchanged, the grinding depth is inversely proportional to the quality of the sub-surface layer. As the stress transfer distance increases, the stress transfer effect gradually decreases. Therefore, the farther away from the surface, the better the quality, and the number of voids formed closer to the processed surface will be more. When the stress is not enough to break the SiC particles, cracks are left in the sub-surface layer of the SiCp/Al composite material. The length of the crack is determined by the distance between the particle location and the machined surface. The longer the distance between the two, the shorter the crack, and vice versa.

Ethics approval and consent to participate

This research project has been approved by the Ethics Committee of Liaoning University of Technology.

Consent for publication

that the work described has not been published before;

that it is not under consideration for publication elsewhere;

that its publication has been approved by all co-authors, if any;

that its publication has been approved by the responsible authorities at the institution where the work is carried out.

The Author agrees to publication in the Journal indicated below and also to publication of the article in English by Springer in Springer's corresponding English-language journal. The copyright to the English-language article is transferred to Springer effective if and when the article is accepted for publication. The author warrants that his/her contribution is original and that he/she has full power to make this grant. The author signs for and accepts responsibility for releasing this material on behalf of anyand all co-authors. The copyright transfer covers the exclusive right to reproduce and distribute the article, including reprints, translations, photographic reproductions, microform, electronic form or any other reproductions of similar nature. After submission of the agreement signed by the corresponding author, changes of authorship or in the order of the authors listed will not be accepted by Springer. Journal: Silicon, chemical samples Names of All contributing authors： Guangyan Guo, Qi Gao, Quanzhao Wang, and Yuanhe Hu.

Availability of data and materials

The data used to support the findings of this study are available from the corresponding author upon request.

Competing interests

The authors have declared that no conflict of interest exists.

Funding

This work was supported by the National Natural Science Foundation of China (No.51775100) and the Doctoral Start-up Fund of Liaoning Province (2019-BS-123).

Authors' contributions

Guo did all the grinding experiments and wrote the papers. Gao guided Guo to revise the paper. Wang made a parameter measurement of the materials used in this experiment. Hu performed regular segmentation of the SiCp/Al composites. All authors read and approved the manuscript.

Acknowledgment

The authors would like to express their gratitude to the reviewers of the manuscript for their valuable suggestions and comments.

Compliance with ethical standards

Authors state that the research was conducted according to ethical standard.

Disclosure of potential conflicts of interest

This research does not involve potential conflicts of interest.

Research involving Human Participants and/or Animals

This research does not involve human participants and animal research.

Informed consent

I solemnly declare that the paper "Study on Meso-scale Grinding Surface Roughness and Sub-surface Quality of High Volume Fraction SiCp/Al2024 composites" presented by us is the result of our research. This paper does not contain any work published or written by any other individual or group, except for the content specifically noted and cited in the paper. I fully realize that the legal consequences of this statement shall be borne by me.

Reference

1. Cui Y (2003) High Volume Fraction SiCp/Al Composites Prepared by Pressureless Melt Infiltration: Processing,

Properties and Applications[J]. Key Engineering Materials, 249:45-48.

2. Zhang Q, Liu D, Chen GQ, Xiu ZY, Wu GH (2009) Performance and application of SiCp/Al composites for electronic packaging[J]. Physical & Failure Analysis of Integrated Circuits. ipfa. ieee International Sympo, 252-255.
3. Lee HS, Jeon KY, Kim HY, Hong SH (2000) Fabrication process and thermal properties of SiCp/Al metal matrix composites for electronic packaging applications[J]. Journal of Materials Science, 35(24):6231-6236.
4. Fan J (2007) Development and Applications of SiCp/Al Composites in Aerospace Field[J]. Materials Review, 21(10):98-101.
5. Shi F, Qian DF, Zhang ZP (2004) Application of SiCp/Al Composite and Its Fabrication by Pressureless Infiltration Technique[J]. Bulletin of the Chinese Ceramic Society, (02):60-65.
6. Yin GQ, Wang D, Cheng J (2019) Experimental investigation on micro-grinding of SiCp/Al metal matrix composites[J]. The International Journal of Advanced Manufacturing Technology, (64):66-78.
7. Sun Y, Su ZP, Gong YD, Ba D, Yin GQ, Zhang H, Zhou LH (2021) Analytical and experimental study on micro-grinding surface-generated mechanism of DD5 single-crystal superalloy using micro-diamond pencil grinding tool[J]. Archives of Civil and Mechanical Engineering, 21(1):1-22.
8. Zhou YG, Gong YD, Cai M, Zhu ZX, Gao Qi, Wen XL (2017) Study on surface quality and subsurface recrystallization of nickel-based single-crystal superalloy in micro-grinding[J]. The International Journal of Advanced Manufacturing Technology, 90(5-8).
9. Zheng W, Liu L, Zhang Q, Zhao JS, Cui GX, Wang Q (2019) Simulation of formation mechanism of machined surface defects in ultrasonic grinding of SiCp/Al composites[J]. Journal of Solid Rocket Technology,42(06):793-800.
10. Zhang CY, Sun Y, Zhao LG (2013) Simulation of single diamond abrasive particle grinding SiCp/Al composites[J]. Tool Engineering, 47(11):15-19.
11. Ma ZF, Liang GX, Zhang H, Tian JJ (2019) Simulation and experimental investigation of high-speed grinding Ti6Al4V with single grain[J]. Tool Engineering,, 53(04):49-53.
12. Wang T , Xie L , Wang X (2015) Simulation study on defect formation mechanism of the machined surface in milling of high volume fraction SiCp/Al composite[J]. The International Journal of Advanced Manufacturing Technology, 79(5-8):1185-1194.
13. Yu X L (2012) Research on precision grinding mechanism and surface evaluation of SiCp/Al composites with high volume fraction[D]. Shenyang University of Technology.
14. Guan JL, Zhu L, Chen L, Ma XQ, Zhang XH (2014) Research on ELID Grinding Efficient Surface Forming Mechanism of SiCp/Al Composites[J]. Advanced Materials Research, 1027:107-110.
15. Wei X, Chen GD, Wang B, Chen GH, Yang L, Tang WM (2021) Characteristics and grinding performance evaluation of the high-fraction GNFs/SiCp/6061Al matrix hybrid composites[J]. Journal of Alloys and Compounds, (29):159049.
16. Sun W, Duan CZ, Yin WD (2021) Chip formation mechanism in machining of Al/SiCp composites based on analysis of particle damage[J]. Journal of Manufacturing Processes, 64:861-877.
17. Huang ST, Zhou L, Yu XL, Xiu LF (2012) Study of the mechanism of ductile-regime grinding of SiCp/Al composites using finite element simulation[J]. International Journal of Materials Research (formerly Zeitschrift fuer Metallkunde), 103(10):1210-1217.
18. Gu P, Zhu CM, Tao Z, Yu YQ (2021) A grinding force prediction model for SiCp/Al composite based on single-abrasive-grain grinding[J]. International Journal of Advanced Manufacturing Technology, 109(5-8).
19. Du JG , Ming WY, Cao Y, Ma J, He WB, Li XK (2019) Particle Removal Mechanism of High Volume Fraction SiCp/Al Composites by Single Diamond Grit Tool[J]. Journal of Wuhan University of Technology-Mater Sci Ed, 34(002):324-331.
20. Zhang FL, Li MC, Wang J, Huang HP, Wang CY, Zhou YM (2020) Effect of arraying parameters on dry grinding performance of patterned monolayer brazed CBN wheel[J]. The International Journal of Advanced Manufacturing Technology, 107(5):2081-2089.
21. Wang YS, Xiu SC, Dong L, Sun C (2016) Study on strengthened layer of workpiece in prestress dry grinding[J]. The International Journal of Advanced Manufacturing Technology, 90(5-8).
22. Qu MN , Jin T, Xie GZ, Cai R,Yi J, Lu AG (2019) Thermal damage control for dry grinding of MgO/CeO2 glass ceramic[J]. International Journal of Advanced Manufacturing Technology, 105(7-8).

23. Johnson GR, Cook WH (1985) Fracture characteristic of three metals subjected to various strains: strains rates, temperature and pressure[J]. Engineering Fracture Mechanics.21(1):31–48.
24. Akbari M, Buhl S, Leinenbach C, Wegener K (2016) A new value for Johnson Cook damage limit criterion in machining with large negative rake angle as basis for understanding of grinding[J]. Journal Materials Processing Technology, 234:58–71.